Publisher: GSA
Journal: GEOL: Geology
DOI:10.1130/G39801.1

# Genesis of the world's largest rare earth element deposit, Bayan Obo, China: protracted mineralization evolution over ~1 billion years

**Wenlei Song[1], Cheng Xu[1*], Martin P. Smith[2], Anton R. Chakhmouradian[3], Marco Brenna[4], Jindřich Kynický[5], Wei Chen[6], Yueheng Yang[7], Miao Deng[1], and Haiyan Tang[8]**

*[1]Key Laboratory of Orogenic Belts and Crustal Evolution, School of Earth and Space Sciences, Peking University, Beijing 100871, China*

*[2]School of Environment and Technology, University of Brighton, Brighton BN24GJ, UK*

*[3]Department of Geological Sciences, University of Manitoba, Manitoba R3T2N2, Canada.*

*[4]Department of Geology, University of Otago, Dunedin 9054, New Zealand*

*[5]Department of Geology and Pedology, Mendel University, Brno 361300, Czech Republic*

*[6]State Key Lab of Geological Processes and Mineral Resources, Wuhan 430074, China University of Geosciences, China*

*[7]Institute of Geology and Geophysics, Chinese Academy of Sciences, Beijing 100029, China*

*[8]College of Earth Science, Jilin University, Changchun 130012, China*

*E-mail: xucheng1999@pku.edu.cn

**ABSTRACT**

The unique, giant, REE deposit at Bayan Obo is the world's largest REE deposit. It is geologically complex and its genesis is still debated. Here, we report in situ Th-Pb dating and Nd isotope ratios for monazite and Sr isotope ratios for dolomite and apatite from fresh drill–cores. The measured monazite ages (361–913Ma) and previously reported whole-rock Sm-Nd data show a linear relationship with initial Nd isotope ratio, suggesting a single-stage evolution from a Sm-Nd source that was formed before 913Ma. All monazites show consistent $\varepsilon Nd_{(1.3Ga)}$ values (0.3 ± 0.6) close to those of the adjacent 1.3Ga carbonatite and mafic dikes. The primary dolomite and apatite show lower $^{87}Sr/^{86}Sr$ ratios (0.7024–0.7030) than the recrystallized dolomite (0.7038–0.7097). The REE ores at Bayan Obo are interpreted to have originally formed as products of ~1.3Ga carbonatitic magmatism and undergone subsequent thermal perturbations induced by Sr-rich, but REE-poor metamorphic fluids derived from nearby sedimentary rocks.

## INTRODUCTION

The rare earth elements (REE) have become the focus of international attention because of their industrial importance to the development of "low carbon" energy and transportation technologies, and because the global REE market is extremely sensitive to geopolitically driven supply limitations (Hatch, 2012). The availability of REE for future markets is a growing concern in the developed world because global demand for these resources is expected to grow significantly (Verplanck and Hitzman, 2016). China, the United States, Russia, Canada, Brazil, Australia, India and Malaysia account for the majority of the world's REE reserves. China presently contains ~40% of the global REE resources (Weng et al., 2015), concentrated primarily in the world's largest REE deposit at Bayan Obo. This deposit has attracted inordinate attention from researchers (over 100 papers in peer-reviewed journals just in the past decade) because of its unparalleled endowment in REE (>100Mt $REE_2O_3$, Weng et al., 2015). The genesis of the Bayan Obo structure and its resources has been the subject of debate for over 50 years. There is no consensus concerning either the age of mineralization (~1300 to ~400Ma; Yang et al., 2017), or the number of mineralization stages (Chao, 1997). Genetic models proposed for Bayan Obo range from sedimentary deposition (Chao, 1997), to metasomatic reworking of metasedimentary marbles by carbonatitic (Smith et al., 1999) or subduction-derived fluids (Yang et al., 2017), to igneous processes related to carbonatite emplacement (Le Bas et al., 2007).

Monazite is one of the principal REE hosts in the Bayan Obo deposit. Here we report integrated, in situ, high-precision Th-Pb ages and Nd isotope ratios of monazite samples from an 1776 m long drill core section from the Bayan Obo deposit. The monazite data were combined with in situ apatite and dolomite isotope analyses to show that the Bayan Obo REE mineralization is of Mid-Mesoproterozoic age and of carbonatitic origin, and shows no evidence of any significant REE contribution from external sources. This Mid-Mesoproterozoic mineralization was subsequently modified by younger thermal events.

## GEOLOGY OF THE DEPOSIT AND SAMPLES

The Bayan Obo deposit is located at the northern margin of the North China Craton (NCC). The basement comprises the Archean Wutai Group (gneisses and migmatites) and Proterozoic Bayan Obo Group. The latter has been subdivided into nine lithological units, conventionally referred to as H1-H9 in ascending chronological order. The Bayan Obo Group is composed predominantly of meta-sandstones and slates, except for the H8 dolomite rock (Fig. DR1 in the GSA Data Repository[1]). Volcanic rocks of trachytic, dacitic and rhyolitic composition, as well as mafic dikes, have been found within the H9 group

Publisher: GSA
Journal: GEOL: Geology
DOI:10.1130/G39801.1

(Zhang et al., 2003; Yang et al., 2011). The metamorphic clastic sequences of the Bayan Obo Group represent sedimentary units deposited within the Bayan Obo pericratonic rift. The REE deposit is hosted by the H8 dolomite rock, which extends for 18km laterally at a width of >1km, and occurs as a spindle-shaped stratiform body. About 100 carbonatite dikes are found adjacent to the deposit, intruding the Bayan Obo Group metasediments (Yang et al., 2011). The REE orebodies consist of disseminated, banded and massive ores, most of which are associated with dolomite, silicates (in particular, alkali clinopyroxene, amphibole and mica), apatite, fluorite and magnetite.

The studied drill core was extracted from the Eastern orebody, within the H8 unit, and has a total length of 1776m. Compared to the H8 unit exposed at the surface, which underwent extensive metasomatic alteration and deformation, and contains abundant aegirine, riebeckite, phlogopite and late-stage fluorite-barite veins superposed over the primary mineral assemblage, the drill samples are relatively fresh. The examined rocks are composed predominantly of fine- to coarse-grained dolomite. Most of the dolomite is euhedral to subhedral, and shows evidence of recrystallization with the development of triple grain junctions. Some of the fine-grained, anhedral dolomites occur as a matrix to the porphyritic dolomites (Fig. DR2), defining a primary, igneous texture. The studied drill core shows significant variations in total light $REE_2O_3$ content, which locally reaches 5.8wt.% (Fig. DR3; Table DR1; for methods, see Data Repository). Textural observations show that the early disseminated monazite was usually partially replaced and overgrown by bastnäsite and apatite (Fig. 1a). Late monazite occurs as monominerallic veinlets, or is associated with bastnäsite veinlets (Fig. 1b). Primary apatite was partially corroded and overgrown by a rim of monazite (Fig. 1c). Recrystallized apatite occurs as veinlets and clusters with bastnäsite (Fig. 1d). The textural evolution of REE minerals indicates extensive metamorphic and metasomatic recrystallization (Smith et al., 1999).

**RESULTS**

The Th-Pb ages were combined with Nd isotopic ratio measurements done independently and in situ on the same monazite grains, to calculate the initial $(^{143}Nd/^{144}Nd)_i$ ratios at the time of formation (Tables DR2,3). These monazites show homogeneous internal textures (Fig. DR4), and have variable ages, ranging from 361 ± 6–913 ± 15Ma. Their corresponding εNd(t) values fall between −6.9 and −18. However, all samples show similar $T_{CHUR}$(Nd) model ages ranging from 1.56 to 1.67Ga, implying derivation from the same source. The inferred ore-forming events at Bayan Obo have been previously constrained chronologically on the basis of whole-rock and mineral assemblages from surface samples, which show a wide range of ages with distinct frequency peaks at ~1.3Ga and ~400Ma (Yang et al., 2017). However, the REE-rich carbonatite dikes adjacent to the orebodies give a consistent Mid-Mesoproterozoic age of ca. 1.3Ga (Fig. 2). The Sm-Nd isochron ages of volcanic rocks and mafic dikes in the Bayan Obo deposit are also close to 1.3Ga. Figure 2 shows the measured monazite ages plotted versus their corresponding εNd(t) values, and provides some of the previously reported Sm-Nd isochron ages and εNd(t) values for reference. Notably, the new and published data show a good correlation, indicating a single-stage Nd isotopic evolution from a single source. Late-stage, magma-derived melts or fluids could serve as a source of REE, but this model would require that the later-emplaced magmas had very low Nd isotopic ratios. This is clearly not the case: all reported Neoproterozoic to Carboniferous igneous rocks in the northern NCC plot above the Nd isotopic evolution line for Bayan

Obo (Fig. 2). Therefore, we infer that late-stage changes in the REE mineralization defined by this evolution line were due to remobilization of these elements from the already existing orebody of Mid-Mesoproterozoic age. This interpretation is supported by textural evidence, such as metasomatic replacement of early monazite and apatite accompanied by the development of new REE minerals (Fig. 1). The trace element and isotope data described below further support the interpretation of the timing of primary REE mineralization.

The origin of the H8 dolomite rock hosting the deposit has been debated. The two “end-member” hypotheses are igneous crystallization from carbonatitic magma (Le Bas et al., 2007) and sedimentary deposition (Chao, 1997). Our Nd isotope evolution line is remarkably different from that characterizing typical sedimentary rocks from units H1-H3, in which the $(^{143}Nd/^{144}Nd)_i$ ratio, calculated from 1.3Ga to 400Ma, is markedly lower than in the REE minerals (Fig. 2). Both dolomite and apatite analyzed in this study show high Sr contents (Table DR4), typical of carbonatitic minerals (Hornig-Kjarsgaard, 1998). Different textural types of dolomite and apatite are characterized by distinct REE distribution patterns (Fig. 3). The primary dolomite shows relatively low REE content (La<10ppm) and a flat distribution pattern with $(La/Yb)_{cn}$ = 1–5. The recrystallized dolomite is characterized by a much more varied and higher REE content (La = 16–109ppm) and stronger enrichment in light REE, with $(La/Yb)_{cn}$ = 8–32. The two generations also differ in their key REE ratios, i.e., the primary variety has higher Eu/Eu* and Y/Ho values relative to the recrystallized dolomite. Early disseminated apatite is significantly enriched in REE (La>1400ppm) and shows a higher Eu/Eu* but lower Y/Ho values than the paragenetically later generation confined to the veinlets (Fig. DR5).

The textural relations and extreme isotopic variability of the Bayan Obo monazite imply that it is a product of dissolution-reprecipitation processes and that its Th-Pb budget was modified over an extended period of time. The extended history of metasomatism at Bayan Obo is recorded in the monazite ages, spanning from 361 to 913Ma. The primary REE mineralization must have formed earlier than 913Ma and may have occurred ca. 1.3Ga, as indicated by the Sm-Nd isochron ages of the ore-bearing H8 unit and spatially associated REE-enriched carbonatites (Fig. 2). These previously studied samples have initial Nd isotopic ratios similar to those of the monazite studied in the present work if calculated for 1.3Ga ($\varepsilon Nd_{1.3Ga} = 0.3 \pm 0.6$), implying a common mantle source. In situ Sr isotopic analysis of the primary dolomite and apatite also gave low $^{87}Sr/^{86}Sr$ values (Table DR5, 0.7024–0.7030), which are far less radiogenic than typical marine carbonates and further support a non-sedimentary origin (Fig. 3). However, the late generations of recrystallized dolomite have variable and high Sr isotopic compositions (0.7038–0.7097). The present-day Sr isotopic ratios measured in the primary dolomite and apatite are considered to approximate the initial $^{87}Sr/^{86}Sr$ values because these minerals contain high levels of Sr, but negligible Rb and thus, are characterized by very low Rb/Sr ratios. Similar initial Sr isotopes (0.7029–0.7030) have been reported from ~1.3Ga carbonatite dikes without contamination by feldspar from the wall rocks in Bayan Obo (Le Bas et al., 2007).

## DISCUSSION AND CONCLUSION

A newly reported zircon age (1301 ± 12Ma) on REE-rich carbonatites at Bayan Obo supports the model of Mid-Mesoproterozoic primary mineralization (Zhang et al., 2017). The $^{87}Sr/^{86}Sr$ ratios of primary dolomite and apatite are close to the Bulk Earth value (0.7029) at 1.3Ga. The $\varepsilon Nd_{1.3Ga}$ value of monazite is also close to the Chondritic

Uniform Reservoir value, implying that the ore-bearing dolomite rock may be derived from a primary, non-depleted mantle source, perhaps residing within the less-accessible parts of the mantle, or in the depleted lithospheric mantle modified by old subducted materials. Experiments show that primary carbonatitic melts derived from carbonated peridotites contain relatively low REE abundances (Foley et al., 2009) and must consequently undergo extensive fractionation in the crust to produce the level of REE enrichment. Initially low REE concentrations in carbonatitic magmas are typically dispersed among such major rock-forming constituents as calcite and apatite (Hornig-Kjarsgaard, 1998), preventing the development of REE mineralization. In contrast, primary carbonatitic magmas can be derived by partial melting of carbonated eclogites (Thomson et al., 2016). In the Trans-North China Orogen of the NCC (i.e., ~300km southeast of Bayan Obo), several occurrences of Paleoproterozoic carbonatite dikes were found to contain high-pressure eclogite xenoliths of recycled crustal origin (Xu et al., 2017a). This discovery provides unambiguous evidence that subducted material is present in the mantle beneath the northern NCC. Seismic imaging of the NCC across the Trans-North China Orogen (Zheng et al., 2009) provides strong support to Paleoproterozoic (1.9–2.1Ga) westward subduction beneath the Western Block of the Craton at the time when it is inferred to have been part of the Columbia supercontinent. Numerous diabase dikes emplaced in the northern NCC (Fig. DR1) are considered to be related to the Mid-Mesoproterozoic breakup of Columbia (see Zhang et al., 2017). The mafic dikes in the northern NCC share geochemical characteristics of both ocean-island basalts and island-arc volcanic rocks, as can be seen in tectonic-setting-based discrimination diagrams (Fig. DR6). Geochemically, these dikes resemble basaltic magmatism whose mantle source was influenced by previous subduction events, and are distinctly different from purely intraplate volcanic rocks in the NCC. In particular, the Bayan Obo mafic dikes and volcanic rocks in unit H9 show consistent negative Nb, Ta and Ti anomalies (normalized to the primary mantle values), and are compositionally similar to arc basalts (Fig. DR7). Crustal contamination as a source of these geochemical deviations can be ruled out because the mafic dikes in the northern NCC show a consistent Nd isotopic signature ($\varepsilon Nd_{1.3Ga}$ = -0.5–1.9; Yang et al., 2011). Therefore, we consider that subduction modification pre-conditioned the mantle source to generate the Bayan Obo carbonatite REE deposit.

Our mineralogical and geochemical results suggest that the primary REE mineralization at Bayan Obo was modified by externally derived fluids, which involved the development of superimposed mineralization and recrystallization of the primary minerals. The metasomatic fluids contain a crustal component, as indicated by a negative shift in Eu/Eu* value and higher $^{87}Sr/^{86}Sr$ ratios in the recrystallized dolomite and apatite (Fig. 3, Fig. DR5). The Y/Ho trends exhibited by dolomite and apatite are mutually complementary, indicating structural controls over Y versus Ho partitioning between crystals and the fluids, whereas both minerals show depletion in Eu with recrystallization. The C-O isotope data from the deposit also show a large variation and plot between mantle and sediment fields (Yang et al., 2017). Moreover, the fluids must have been poor in REE, but rich in Sr to explain the positive $^{87}Sr/^{86}Sr$ excursion. Caledonian subducted slab-derived fluids, as proposed by Yang et al. (2017), are unlikely to be responsible for the observed geochemical trends, because such fluids would be expected to have radiogenic Nd isotopes (Xu et al., 2017b). Their interaction with the H8 unit would inevitably modify its Nd isotopic signature, causing deviation of monazite εNd(t) values from the continuous evolutionary line shown in Figure 2. Moreover, the Neoproterozoic to Carboniferous magmatism in the northern NCC could not provide fluids sufficiently depleted in radiogenic Nd to explain the low negative εNd(t) values of young Bayan Obo monazite generations. The sedimentary rocks present in the sequence at Bayan Obo are a viable alternative source of metasomatizing fluids. These rocks show elevated Sr levels (up to 580ppm) coupled with a strongly radiogenic Sr isotopic signature ($^{87}Sr/^{86}Sr_{(985Ma)}$=0.7147), but are poor in REE (Zhang et al., 2003), and may have contributed this signature to the post-ore metasomatic fluids involved in dolomite and apatite recrystallization. These sedimentary rocks underwent metamorphism to various degrees (from greenschist to low amphibolites facies conditions) and could serve as a persistent fluid source responsible for textural and geochemical changes in the H8 dolomite rock.

In conclusion, our interpretation of the isotopic and trace element characteristics of monazite, dolomite and apatite support the derivation of primary REE from a Mid-Mesoproterozoic carbonatitic source. The apparent discrepancy in the behavior of Sr and Nd isotopes highlights the importance of multi-systemic approach to geologically complex mineral deposits, and reflects a protracted history of metasomatism induced by Sr-rich, REE-poor fluids. In a similar case, the Nolans Bore REE deposit in Australia has been found to have experienced multiple episodes of recrystallization/internal reworking over a period of at least 1 billion years after primary ore formation (Schoneveld et al., 2015). The resetting of the ore system may be common in most REE deposits, and may be critical in the high grade of some deposits. Interpreting geochronological results from the

REE orebodies should be undertaken with caution. However, with the utilization of petrographic constrained analyses, recrystallization processes may be related to regional tectonic events, and therefore complex REE orebodies could be used to unravel their tectonic evolution.

## ACKNOWLEDGMENTS

This research was financially supported by Chinese NSF (41573033; 41688103; 41773022). We are particularly grateful to Carl Spandler, Philip L Verplanck and Franco Pirajno for their constructive comments, and J. Brendan Murphy for handling our paper.

## REFERENCES CITED

Chao, E.C.T., 1997, The sedimentary carbonate-hosted giant Bayan Obo REE-Fe-Nb ore deposit of Inner Mongolia, China: A corner stone example for giant polymetallic ore deposits of hydrothermal origin: U.S. Geological Survey Bulletin, v. 2143, p. 1–65.

Foley, S.F., Yaxley, G.M., Rosenthal, A., Buhre, S., Kiseeva, E.S., Rapp, R.P., and Jacob, D.E., 2009, The composition of near-solidus melts of peridotite in the presence of $CO_2$ and $H_2O$ between 40 and 60 kbar: Lithos, v. 112, p. 274–283, https://doi.org/10.1016/j.lithos.2009.03.020.

Hatch, G.P., 2012, Dynamics in the global market for rare earths: Elements, v. 8, p. 341–346, https://doi.org/10.2113/gselements.8.5.341.

Hornig-Kjarsgaard, I., 1998, Rare earth elements in sovitic carbonatites and their mineral phases: Journal of Petrology, v. 39, p. 2105–2121, https://doi.org/10.1093/petrology/39.11.2105.

Le Bas, M.J., Yang, X.M., Taylor, R.N., Spiro, B., Milton, J.A., and Zhang, P.S., 2007, New evidence from a calcite-dolomite carbonatite dike for the magmatic origin of the massive Bayan Obo ore-bearing dolomite marble, Inner Mongolia, China: Mineralogy and Petrology, v. 90, p. 223–248, https://doi.org/10.1007/s00710-006-0177-x.

Schoneveld, L., Spandler, C., and Hussey, K., 2015, Genesis of the central zone of the Nolans Bore rare earth element deposit, Northern Territory, Australia: Contributions to Mineralogy and Petrology, v. 170, p. 11, https://doi.org/10.1007/s00410-015-1168-x.

Shao, J.A., Hong, D.W., and Zhang, L.Q., 2002, Genesis of Sr-Nd isotopic characteristics of igneous rocks in Inner Mongolia: Geological Bulletin of China, v. 21, p. 817–822.

Smith, M.P., Henderson, P., and Zhang, P., 1999, Reaction relationships in the Bayan Obo Fe-REE-Nb deposit, Inner Mongolia, China: Implications for the relative stability of rare-earth element phosphates and fluorocarbonates: Contributions to Mineralogy and Petrology, v. 134, p. 294–310, https://doi.org/10.1007/s004100050485.

Thomson, A.R., Walter, M.J., Kohn, S.C., and Brooker, R.A., 2016, Slab melting as a barrier to deep carbon subduction: Nature, v. 529, p. 76–79, https://doi.org/10.1038/nature16174.

Verplanck, P.L., and Hitzman, M.W., 2016, Introduction: Rare earth and critical elements in ore deposits: Economic Geology and the Bulletin of the Society of Economic Geologists, v. 18, p. 1–4.

Weng, Z., Jowitt, S.M., Mudd, G.M., and Haque, N., 2015, A detailed assessment of global rare earth element resources: Opportunities and challenges: Economic Geology and the Bulletin of the Society of Economic Geologists, v. 110, p. 1925–1952, https://doi.org/10.2113/econgeo.110.8.1925.

Xu, C., Kynicky, J., Smith, M.P., Kopriva, A., Brtnicky, M., Urubek, T., Yang, Y.H., Zhao, Z., He, C., and Song, W., 2017b, Origin of heavy rare earth mineralization in South China: Nature Communications, v. 8, p. 14598, https://doi.org/10.1038/ncomms14598.

Xu, C., Kynicky, J., Tao, R.B., Liu, X., Zhang, L.F., Pohanka, M., Song, W.L., and Fei, Y.W., 2017a, Recovery of an oxidized majorite inclusion from Earth's deep asthenosphere: Science Advances, v. 3, p. e1601589, https://doi.org/10.1126/sciadv.1601589.

Yang, K.F., Fan, H.R., Santosh, M., Hu, F.F., and Wang, K.Y., 2011, Mesoproterozoic mafic and carbonatitic dikes from the northern margin of the North China Craton: Implications for the final breakup of Columbia supercontinent: Tectonophysics, v. 498, p. 1–10, https://doi.org/10.1016/j.tecto.2010.11.015.

Yang, X., Lai, X., Pirajno, F., Liu, Y., Ling, M., and Sun, W., 2017, Genesis of the Bayan Obo Fe-REE-Nb formation in Inner Mongolia, North China Craton: A perspective review: Precambrian Research, v. 288, p. 39–71, http://doi.org/10.1016/j.precamres.2016.11.008.

Zhang, S.H., Zhao, Y., and Liu, Y., 2017, A precise zircon Th-Pb age of carbonatite sills from the world's largest Bayan Obo deposit: Implications for timing and genesis of REE-Nb mineralization: Precambrian Research, v. 291, p. 202–219, http://dx.doi.org/10.1016/j.precamres.2017.01.024.

Zhang, Z.Q., Yuan, Z.X., Tang, S.H., Bai, G., and Wang, J.H., 2003, Age and Geochemistry of the Bayan Obo Ore Deposit: Beijing, Geological Publishing House, 222 p.

Zheng, T., Zhao, L., and Zhu, R., 2009, New evidence from seismic imaging for subduction during assembly of the North China craton: Geology, v. 37, p. 395–398, https://doi.org/10.1130/G25600A.1.

Zhu, X.K., Sun, J., and Pan, C., 2015, Sm-Nd isotopic constraints on rare-earth mineralization in the Bayan Obo ore deposit, Inner Mongolia, China: Ore Geology Reviews, v. 64, p. 543–553, https://doi.org/10.1016/j.oregeorev.2014.05.015.

## FIGURE CAPTIONS

Figure 1. Back-scattered-electron images showing the characteristic mineral assemblages and textures observed in the Bayan Obo drill core. Dol, dolomite; Mnz, monazite; Ap, apatite; Bas, bastnäsite; Mag, magnetite.

Figure 2. Trend of Nd isotopic evolution of Bayan Obo monazite with age compared to other relevant isotopic data. The dashed line is the trend line of the monazite and can be extended to 1.3Ga, where the εNd(t) value is close to zero and similar to the εNd(t) values of the H8 unit (Zhang et al., 2003; Zhu et al., 2015; Yang et al., 2017), mafic dikes (Yang et al., 2011) and volcanic rocks (Zhang et al., 2003) within the H9 unit, and carbonatite dikes adjacent to the deposit (Zhang et al., 2003; Le Bas et al., 2007; Yang et al., 2011). Data for sedimentary rocks (Zhang et al., 2003) from Bayan Obo and igneous rocks (Shao et al., 2002) from the northern NCC are plotted.

Figure 3. Chondrite-normalized REE patterns and $^{87}Sr/^{86}Sr$ ratios of dolomite and apatite from the drill core. Average REE abundances were used with error bars of one standard deviation.

[1]GSA Data Repository item 2018xxx, methods, figures, and tables, is available online at http://www.geosociety.org/datarepository/2018/ or on request from editing@geosociety.org.

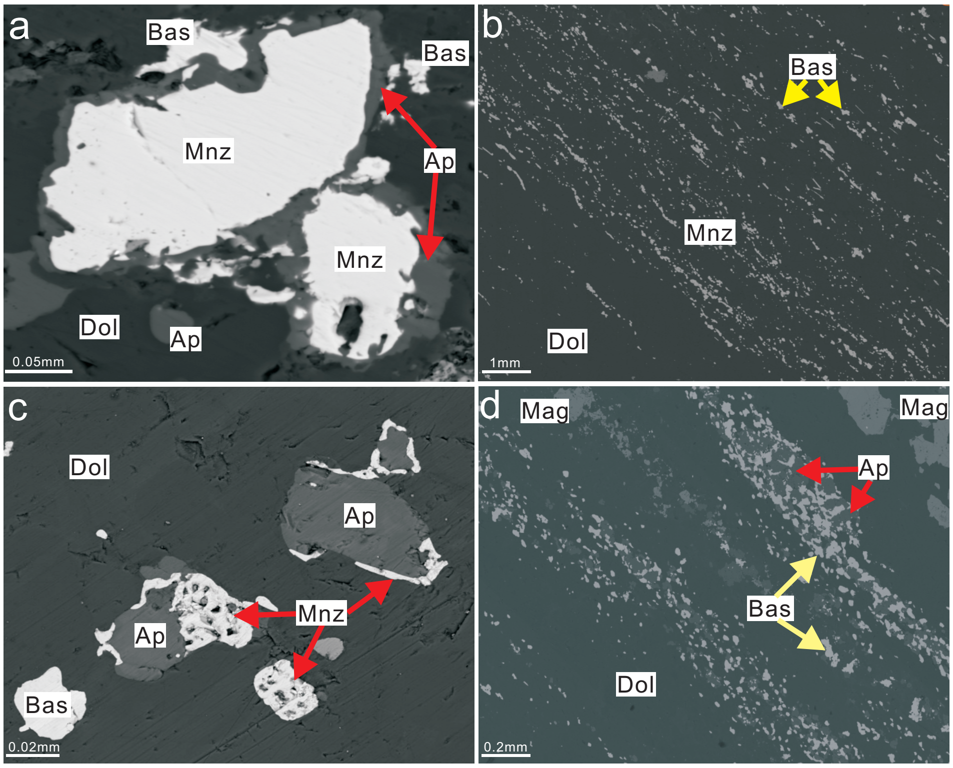
a
Bas
Bas
Mnz
Ap
Mnz
Dol
Ap
0.05mm
b
Bas
Mnz
Dol
1mm
c
Dol
Ap
Mnz
Ap
Bas
0.02mm
d
Mag
Mag
Ap
Bas
Dol
0.2mm

Figure 1

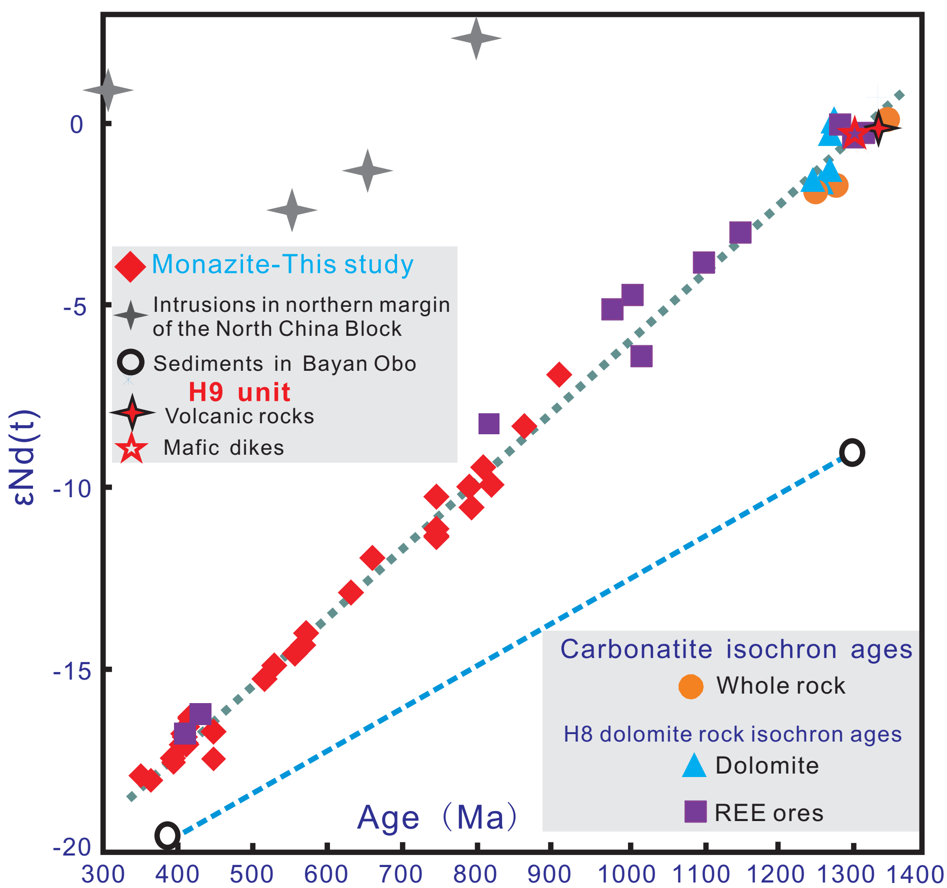

Monazite-This study
Intrusions in northern margin of the North China Block
Sediments in Bayan Obo
H9 unit
Volcanic rocks
Mafic dikes
Carbonatite isochron ages
Whole rock
H8 dolomite rock isochron ages
Dolomite
REE ores
εNd(t)
0
-5
-10
-15
-20
Age（Ma）
300
400
500
600
700
800
900
1000
1100
1200
1300
1400


Figure 2

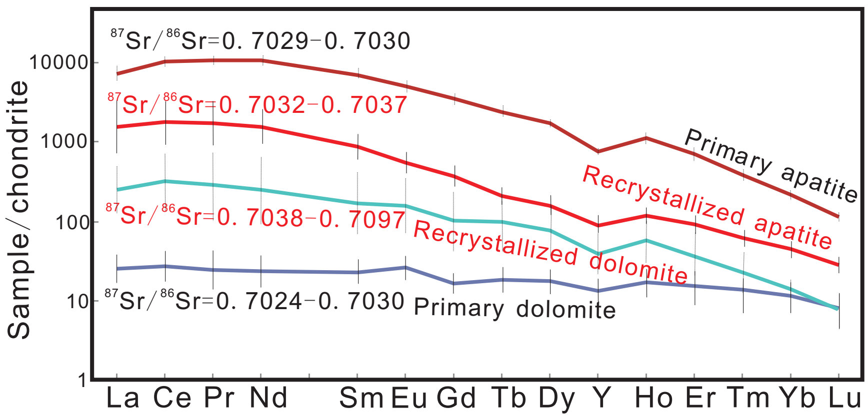

Sample/chondrite
10000
1000
100
10
1
87Sr/86Sr=0. 7029–0. 7030
87Sr/86Sr=0. 7032–0. 7037
87Sr/86Sr=0. 7038–0. 7097 Recrystallized dolomite
87Sr/86Sr=0. 7024–0. 7030 Primary dolomite
Primary apatite
Recrystallized apatite
La Ce Pr Nd Sm Eu Gd Tb Dy Y Ho Er Tm Yb Lu


Figure 3

GSA Data Repository 2018XXX

W. Song, C. Xu*, M.P. Smith, A.R. Chakhmouradian, M. Brenna, J. Kynický, W. Chen, Y. Yang, M. Deng, and H. Tang, 2018, Genesis of the world's largest rare earth element deposit, Bayan Obo, China: protracted mineralization evolution over ~1 billion years: Geology

## Analytical Methods

### Whole-rock analysis

Major and rare earth element abundances in drill core samples were determined by a Spectro Blue Sop inductively coupled plasma optical emission spectrometer (ICP-OES) at the School of Earth and Space Sciences, Peking University. The analytical precision is ±5% for all the elements.

### Element mapping

Compositional X-ray maps of monazites were obtained with an Oxford INCA X-MAX50 250+, energy dispersive X-ray spectrometer installed on a FEI Quanta-650FEG scanning electron microscope, at the School of Earth and Space Sciences, Peking University. The backscattered electron and energy-dispersive X-ray data acquired from the samples were combined and processed automatically to generate the most sensitive X-ray mapping. The sample, coated with a conductive Cr layer (10 nm thickness) to prevent sample charging, was analyzed in a high-vacuum mode at standard operating conditions (accelerating voltage of 20 kV, probe current 5 nA).

## Monazite dating

Monazite grains ranging from 50 to 100 μm across were collected from the drill core using conventional heavy liquid separation techniques. Back-scattered electron images show that the crystals are compositionally homogeneous and free of inclusions. The Th-Pb dating of monazite was performed using a Cameca IMS-1280 secondary-ion mass-spectrometer (SIMS) at the Institute of Geology and Geophysics (IGG), Chinese Academy of Sciences (CAS). During the analysis, an $O^{2-}$ primary ion beam was accelerated at 13 kV with an intensity of ca. 2-3 nA. Aperture illumination mode (Kohler illumination) was used with a 200-μm primary beam mass filter aperture to produce even sputtering over the entire analyzed area. The ellipsoidal spot was about 20 × 30 μm in size. Positive secondary ions were extracted with a 10 kV potential. Monazite 44069 was used as a standard. A $^{207}$Pb-based common Pb correction method was used. Further instrumental and analytical details can be found in Li et al. (2013).

## Trace element analysis

In-situ laser-ablation analyses of dolomite and apatite in thin sections were performed by inductively-coupled-plasma mass-spectrometry (ICP-MS) at the School of Earth and Space Sciences, Peking University, using a COMPexPro

102 excimer laser and an Agilent7500ce/cs mass-spectrometer. The diameter of an ablation spot was 32 μm. The NIST 610 glass was used as a calibration standard, and the Ca content measured by electron-microprobe analysis, as an internal standard. Signal intensity for indicative trace elements was monitored online during the analysis to ensure that the ablation spot was confined to the area of interest and did not sample other mineral phases or inclusions. The analytical error was estimated to be better than 5% at the ppm level.

**Nd-Sr isotopic analysis**

The Nd isotopic composition of monazite was measured in situ by multi-collector ICP-MS using a Thermo-Finnigan Neptune instrument coupled to a 193-nm ArF excimer laser-ablation system at the IGG, CAS. The diameter of a laser spot and frequency were adjusted to between 10-24 μm and 4-10 Hz, respectively, depending on the Nd concentration in the sample. Each spot analysis consisted of approximately 60 s of signal acquisition. More detailed information on the in-situ Nd isotopic analysis employed in the present work is available in Yang et al. (2008). The Sr isotopic compositions of dolomite and apatite were measured in situ by laser-ablation multicollector ICP-MS (Resonics + Nu instruments) at the State Key Laboratory of Geological Processes and Mineral Resources, China University of Geosciences (Wuhan). The isotopic ratios were quantified in a static multicollector mode at low resolution, using seven Faraday collectors and a mass configuration array from $^{82}Kr$ to $^{88}Sr$ to monitor variations in Kr, Rb and Sr signals. The detailed analytical procedure and data-reduction strategy are described in Tong et al. (2015).

## Figure captions for Data Repository

Figure DR1. Geological sketch map of the Bayan Obo deposit. a: The locations of Bayan Obo and ~1.3 Ga mafic dikes in the northern North China Craton (NCC; Yang et al., 2011; Zhang et al., 2012; Wang et al., 2014); b: The locations of drill core, carbonatite and mafic dikes in Bayan Obo.

Figure DR2. Drill core samples and their photomicrographs. a, b: Drill cores collected from the Eastern Orebody at a depth of 1776 m. c: Photomicrograph of dolomite (Dol) showing re-crystallization texture with the development of elongation and preferred orientation, and triple junctions between crystals. Rare earth minerals (REM) of monazite and REE-fluorocarbonates occur as veinlets. d: Photomicrograph of primary fine-grained dolomite as a matrix to porphyritic dolomite. Disseminated REM is associated with fluorite (Fl).

Figure DR3. Plot showing the total light $REE_2O_3$ contents (La-Sm) of the drill core samples with vertical depth.

Figure DR4. X-ray compositional maps of representative monazite grains.

Figure DR5. Compositional variation of primary and recrystallized dolomite (Dol) and apatite (Ap) from the Bayan Obo drill cores. a: $La/Yb_{cn}$ (cn -

chondrite normalized) vs. total REE; b: Y/Ho vs. Eu/Eu* (Eu anomaly).

Figure DR6. Revised tectonic discrimination diagrams for mafic dikes from the northern NCC. Data of the Wulahada and Wudalianchi volcanic fields in NCC are plotted as reference for cases of basaltic magmatism with the source influenced by previous subduction events (Wulahada at 142 Ma; Zhang et al., 2003) and for purely intraplate (OIB-like) volcanism from an enriched source (Wudalianchi at 10 Ma to recent; Zhang et al., 1995). The Mid-Mesoproterozoic mafic dikes (Zhang et al., 2012; Wang et al., 2014) in northern NCC plot in both IAB and OIB, and Bayan Obo data (Wang et al., 2003; Yang et al., 2011) mostly in the IAB field, indicating influence of subduction derived fluids in their mantle source. The tectonic discrimination diagrams are from Vermeesch (2006). OIB, Ocean Island Basalt; IAB, Island Arc Basalt; MORB, Middle Ocean Ridge Basalt.

Figure DR7. Primitive mantle normalized diagram for mafic dikes from the northern NCC. Data of OIB is from Sun and McDonough (1989), IAB based on average compositions reported by Jakes and Gill (1970), McCulloch and Gamble, (1991), and with dashed Ta abundance based on the Nb/Ta ratios reported by Stolz et al. (1996). Additional data sources are same as Fig. DR6. Note that the Bayan Obo mafic rocks have Nb, Ta and Ti negative anomalies and Pb and Sr positive anomalies resembling IAB, and have mostly lower elemental abundances than OIB, suggesting a subduction influence in their genesis.

## References for Data Repository


Jakes, P., and Gill, J., 1970, Rare earth elements and the island arc tholeiitic series: Earth and Planetary Science Letters, v. 9, p. 17-28.

Li, Q.L., Li, X.H., Lan, Z.W., Guo, C.L., Yang, Y.N., Liu, Y., and Tang, G.Q., 2013, Monazite and xenotime U-Th-Pb geochronology by ion microprobe: dating highly fractionated granites at Xihuashan tungsten mine, SE China: Contributions to Mineralogy and Petrology, v. 166, p. 65-80.

McCulloch, M.T., and Gamble, J., 1991, Geochemical and geodynamical constraints on subduction zone magmatism: Earth and Planetary Science Letters, v. 102, p. 358-374.

Stolz, A., Jochum, K., Spettel, B., and Hofmann, A., 1996, Fluid-and melt-related enrichment in the subarc mantle: evidence from Nb/Ta variations in island-arc basalts: Geology, v. 24, p. 587-590.

Sun, S.-S., and McDonough, W.F., 1989, Chemical and isotopic systematics of oceanic basalts: implications for mantle composition and processes: Geological Society, London, Special Publications 42, p. 313-345.

Tong, X.R., Liu, Y., Hu, Z., Chen, H., Zhou, L., Hu, Q., Xu, R., Deng, L., Chen, C., and Gao, S., 2015, Accurate Determination of Sr Isotopic Compositions in Clinopyroxene and Silicate Glasses by LA-MC-ICP-MS: Geostandards and Geoanalytical Research, v. 40, p. 85-89.

Vermeesch, P., 2006, Tectonic discrimination diagrams revisited: Geochemistry Geophysics Geosystems, v. 7, p. Q06017.

Wang, Q.H., Yang, H., Yang, D.B., and Xu, W.L., 2014, Mid-Mesoproterozoic (~ 1.32 Ga) diabase swarms from the western Liaoning region in the northern margin of the North China Craton: Baddeleyite Pb–Pb geochronology, geochemistry and implications for the final breakup of the Columbia supercontinent: Precambrian Research, v. 254, p. 114-128.

Wang, Y., Qiu, Y., Gao, J., and Zhang, Q., 2003, Proterozoic anorogenic magmatic rocks and their constraints on mineralizations in the Bayan Obo deposit region, Inner Mongolia: Science in China (D), v. 46, p. 26-40.

Yang, K.F., Fan, H.R., Santosh, M., Hu, F.F., and Wang, K.Y., 2011, Mesoproterozoic mafic and carbonatitic dykes from the northern margin of the North China Craton: implications for the final breakup of Columbia supercontinent: Tectonophysics, v. 498, p. 1-10.

Yang, Y.H., Sun, J.F., Xie, L.W., Fan, H.R., and Wu, F.Y., 2008, In situ Nd isotopic measurement of natural geological materials by LA-MC-ICPMS: Chinese Science Bulletin, v. 53, p. 1062-1070.

Zhang, H.F., Sun, M., Zhou, X.H., Zhou, M.F., Fan, W.M., and Zhang, J.P., 2003, Secular evolution of the lithosphere beneath the eastern North China Craton: evidence from Mesozoic basalts and high-Mg andesites: Geochimica et Cosmochimica Acta, v. 67, p. 4373-4387.

Zhang, M., Suddaby, P., Thompson, R.N., Thirlwall, M.F., and Menzies, M.A., 1995, Potassic volcanic rocks in NE China: geochemical constraints on mantle source and magma genesis: Journal of Petrology, v. 36, p. 1275-1303.

Zhang, S.H., Zhao, Y., and Santosh, M., 2012, Mid-Mesoproterozoic bimodal magmatic rocks in the northern North China Craton: implications for magmatism related to breakup of the Columbia supercontinent: Precambrian Research, v. 222-223, p. 339-367.

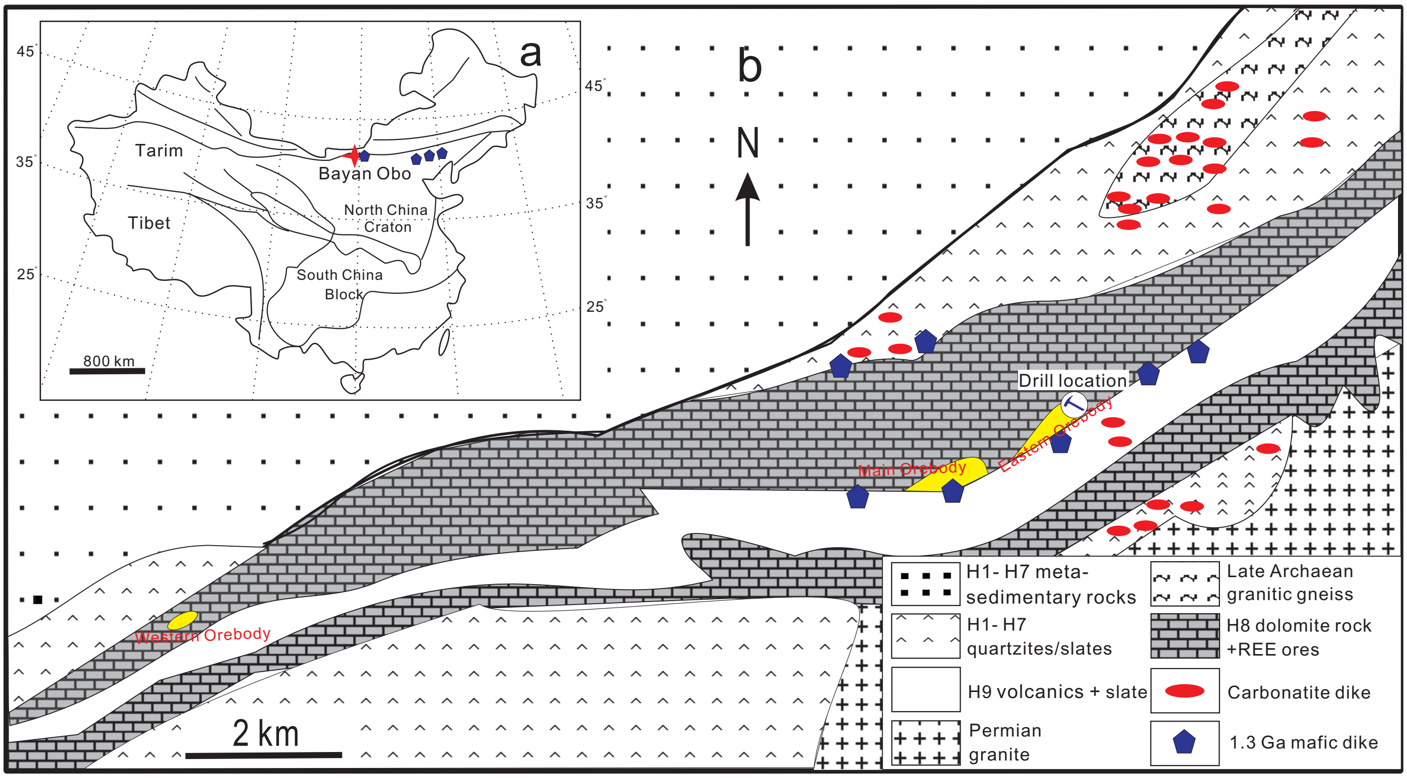

a
45°
35°
25°
45°
35°
25°
Tarim
Tibet
Bayan Obo
North China
Craton
South China
Block
800 km
b
N
Drill location
Main Orebody
Eastern Orebody
Western Orebody
2 km
H1- H7 meta-
sedimentary rocks
Late Archaean
granitic gneiss
H1- H7
quartzites/slates
H8 dolomite rock
+REE ores
H9 volcanics + slate
Carbonatite dike
Permian
granite
1.3 Ga mafic dike


Figure DR1

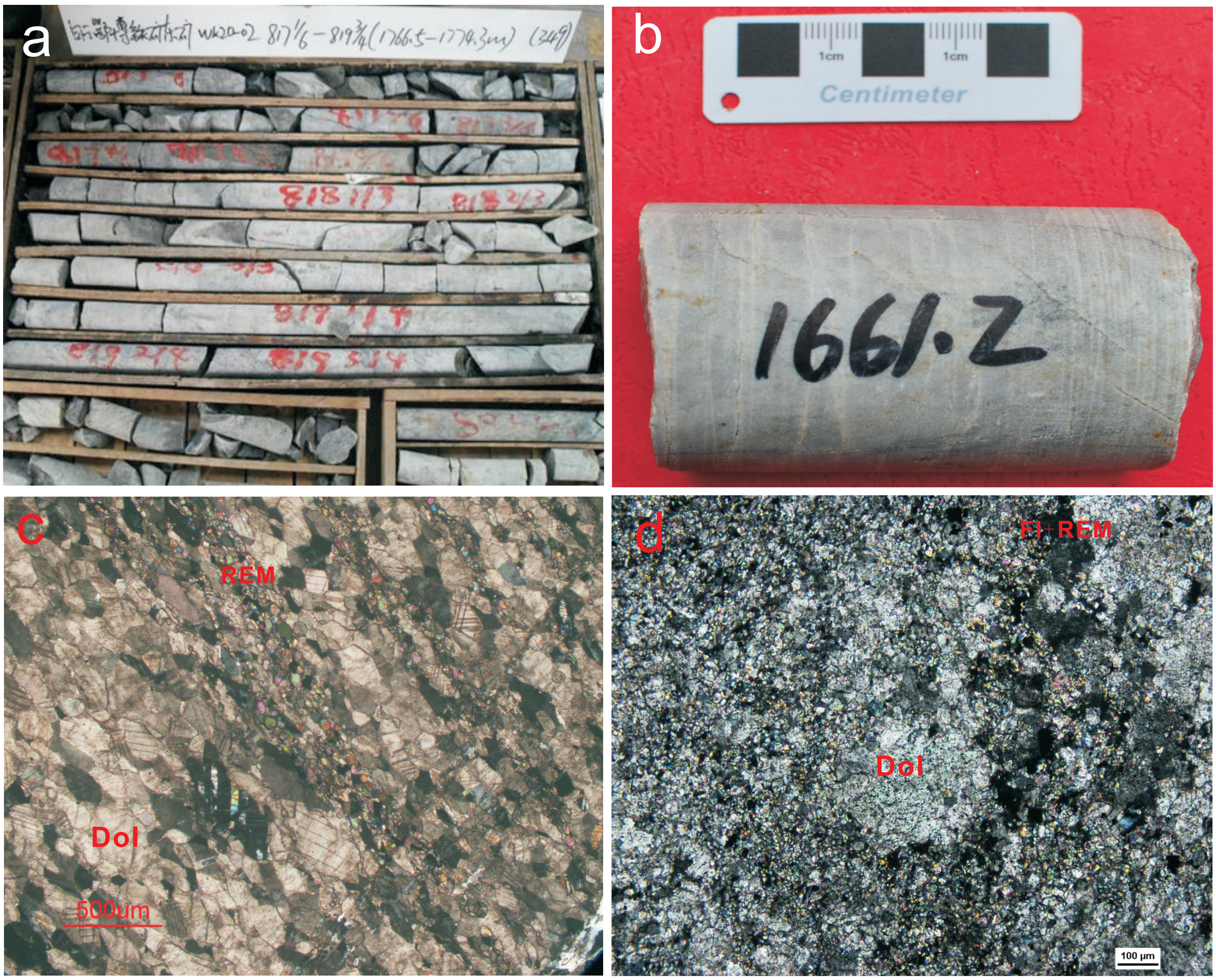


Figure DR2

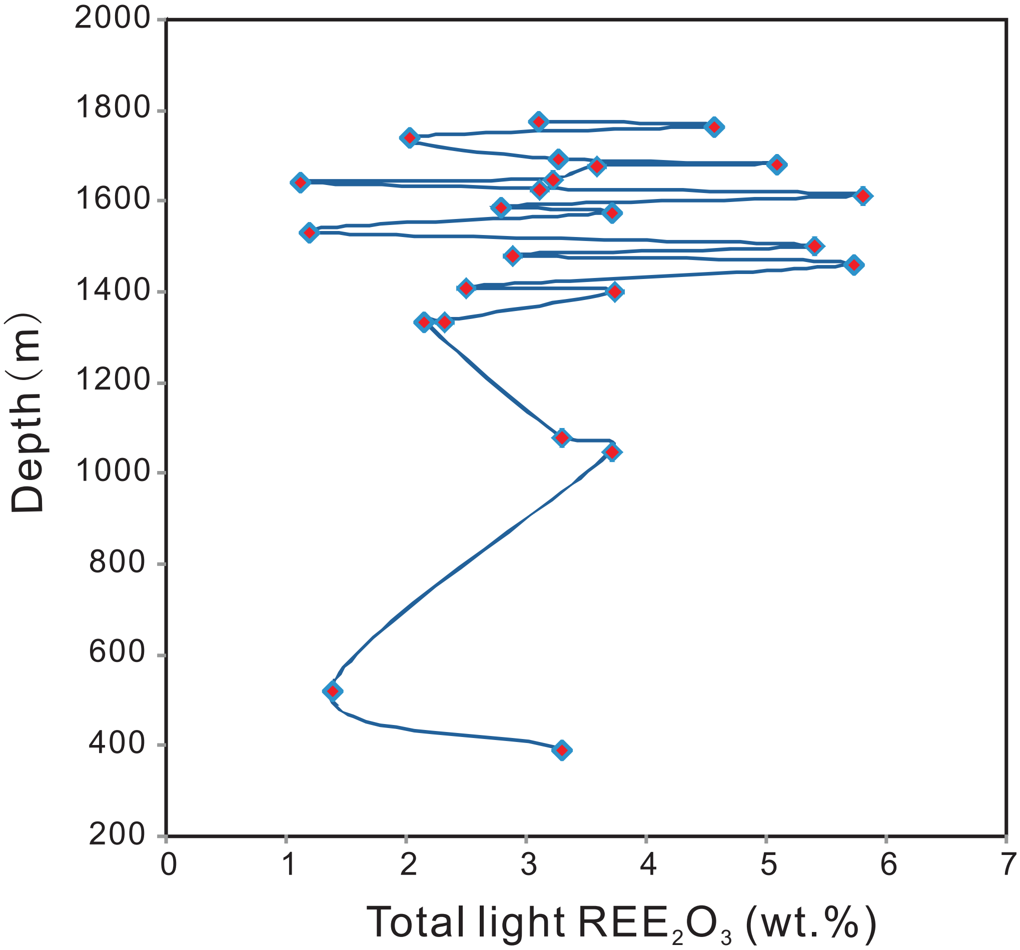
2000
1800
1600
1400
1200
1000
800
600
400
200
Depth (m)
0
1
2
3
4
5
6
7
Total light $REE_2O_3$ (wt.%)

Figure DR3

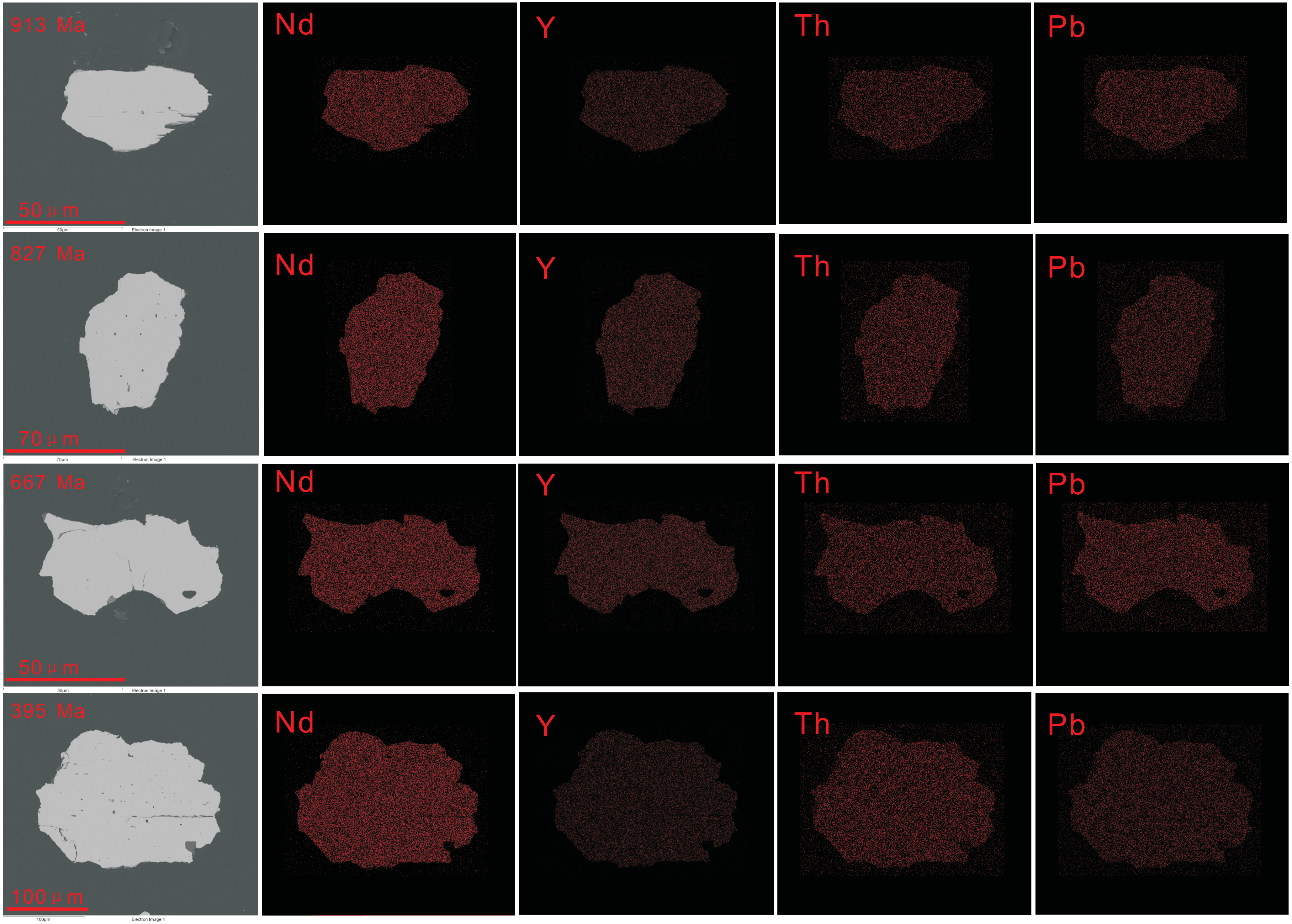
913 Ma
Nd
Y
Th
Pb
50 μ m
827 Ma
Nd
Y
Th
Pb
70 μ m
667 Ma
Nd
Y
Th
Pb
50 μ m
395 Ma
Nd
Y
Th
Pb
100 μ m

Figure DR4

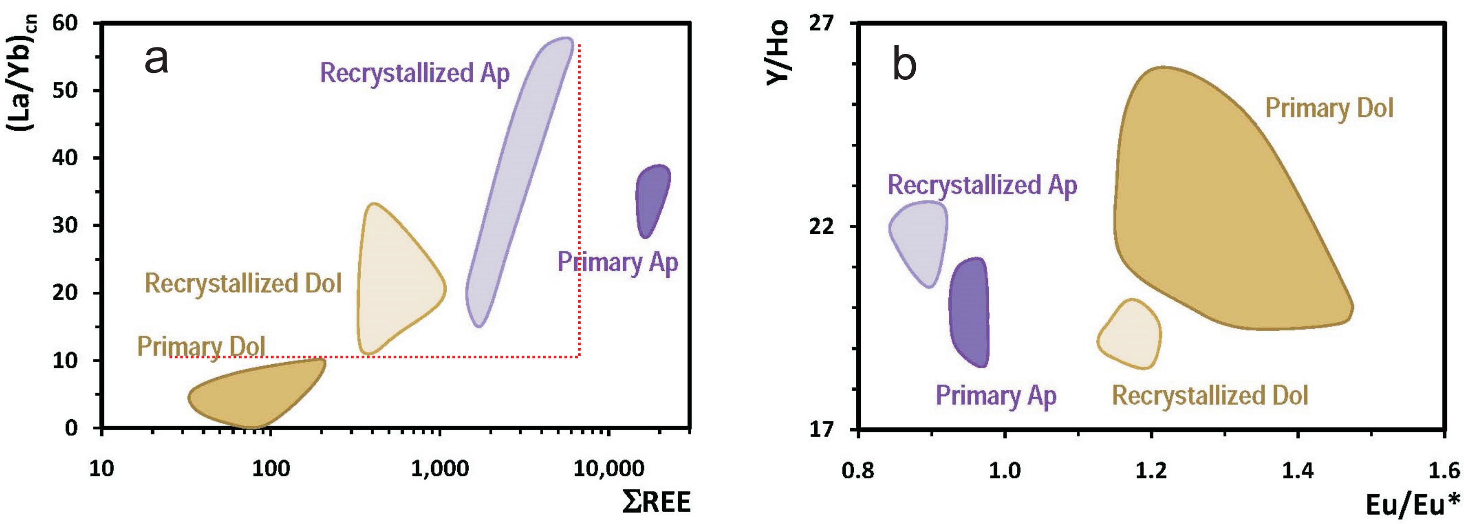

a
Recrystallized Ap
Primary Ap
Recrystallized Dol
Primary Dol
(La/Yb)cn
60
50
40
30
20
10
0
10
100
1,000
10,000
ΣREE
b
Primary Dol
Recrystallized Ap
Primary Ap
Recrystallized Dol
Y/Ho
27
22
17
0.8
1.0
1.2
1.4
1.6
Eu/Eu*


Figure DR5

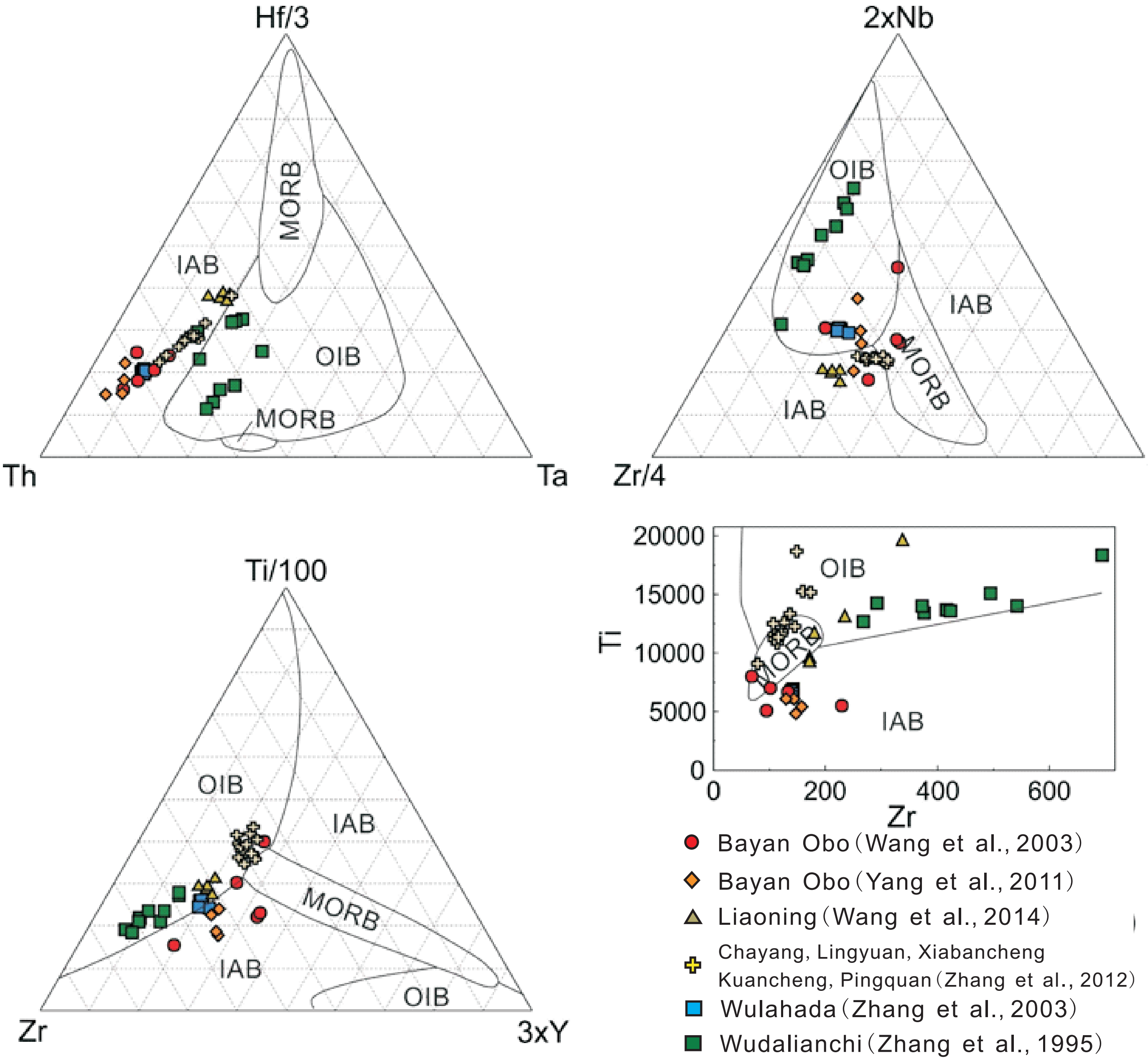

Hf/3
MORB
IAB
OIB
MORB
Th
Ta
2xNb
OIB
IAB
MORB
IAB
Zr/4
Y
Ti/100
OIB
IAB
MORB
IAB
OIB
Zr
3xY
20000
15000
10000
5000
0
Ti
OIB
MORB
IAB
0
200
400
600
Zr
Bayan Obo (Wang et al., 2003)
Bayan Obo (Yang et al., 2011)
Liaoning (Wang et al., 2014)
Chayang, Lingyuan, Xiabancheng
Kuancheng, Pingquan (Zhang et al., 2012)
Wulahada (Zhang et al., 2003)
Wudalianchi (Zhang et al., 1995)


Figure DR6

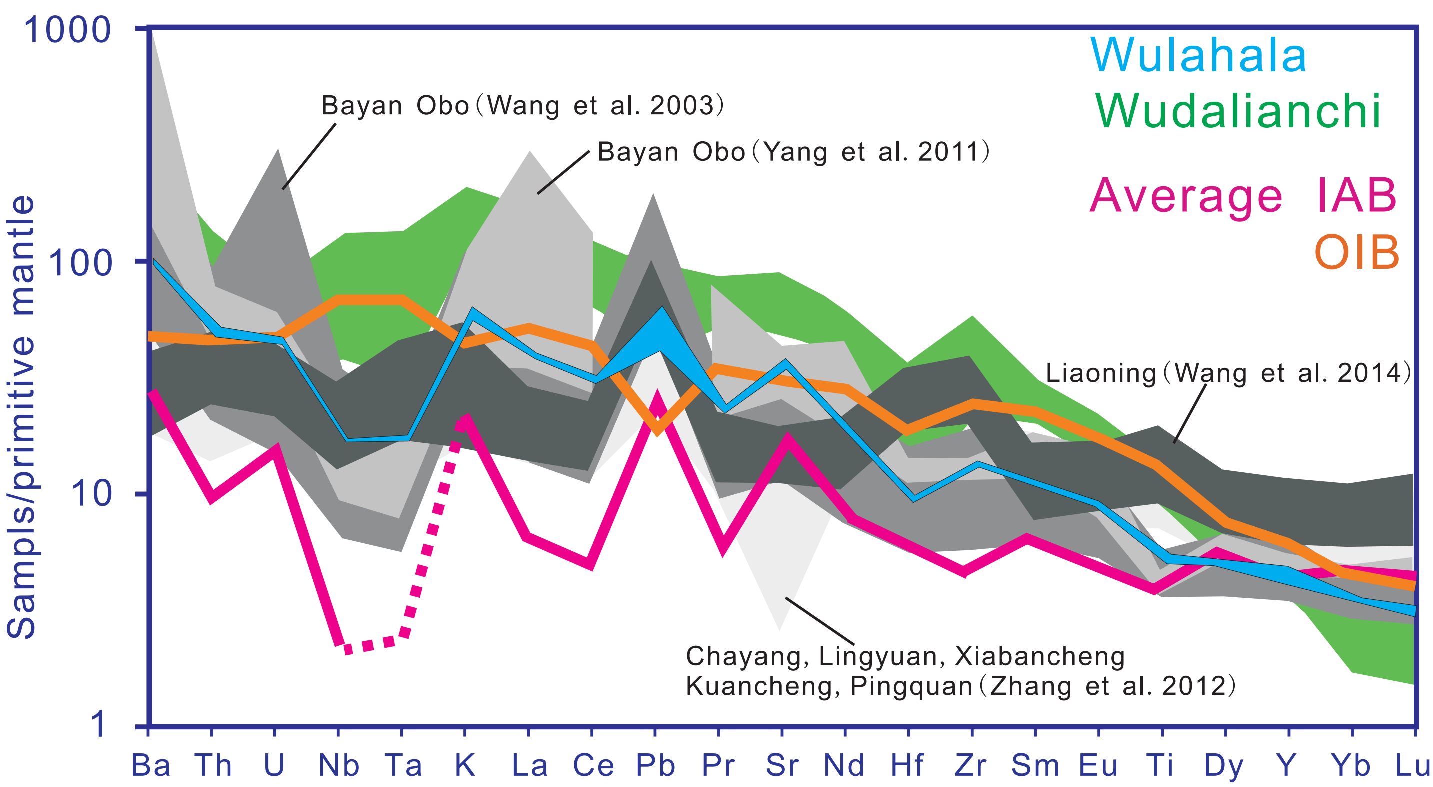

1000
100
10
1
Sampls/primitive mantle
Wulahala
Wudalianchi
Average IAB
OIB
Bayan Obo（Wang et al. 2003）
Bayan Obo（Yang et al. 2011）
Liaoning（Wang et al. 2014）
Chayang, Lingyuan, Xiabancheng
Kuancheng, Pingquan（Zhang et al. 2012）
Ba Th U Nb Ta K La Ce Pb Pr Sr Nd Hf Zr Sm Eu Ti Dy Y Yb Lu


Figure DR7

Table DR1. Chemical compositions (wt.%) in Bayan Obo drill cores with different depths

| Depth(m) | $TiO_2$ | $Al_2O_3$ | FeO | MgO | CaO | MnO | $Na_2O$ | $K_2O$ | $P_2O_5$ | BaO | SrO | $La_2O_3$ | $Ce_2O_3$ | $Pr_2O_3$ | $Nd_2O_3$ | $Sm_2O_3$ |
|---|---|---|---|---|---|---|---|---|---|---|---|---|---|---|---|---|
| 392 | 0.03 | 0.06 | 17.20 | 13.53 | 30.91 | 4.30 | 0.08 | 0.04 | 0.04 | 0.07 | 0.26 | 0.67 | 1.67 | 0.21 | 0.68 | 0.06 |
| 520 | 0.06 | 0.03 | 6.55 | 18.65 | 32.03 | 1.77 | 0.07 | 0.02 | 0.23 | 0.44 | 0.52 | 0.36 | 0.69 | 0.08 | 0.24 | 0.02 |
| 1048 | 0.08 | 0.98 | 12.23 | 13.44 | 24.58 | 2.35 | 1.81 | 1.72 | 0.31 | 0.05 | 0.63 | 0.93 | 2.07 | 0.20 | 0.47 | 0.03 |
| 1080 | 0.05 | 1.59 | 7.69 | 13.89 | 27.33 | 2.72 | 0.04 | 1.89 | 1.85 | 0.20 | 0.23 | 0.59 | 1.55 | 0.22 | 0.84 | 0.09 |
| 1336 | 0.04 | 0.14 | 7.74 | 14.62 | 31.25 | 2.60 | 0.08 | 0.06 | 1.97 | 0.99 | 0.31 | 0.57 | 1.05 | 0.12 | 0.37 | 0.03 |
| 1336 | 0.04 | 0.06 | 7.74 | 14.62 | 31.25 | 1.76 | 0.08 | 0.01 | 2.54 | 0.15 | 0.46 | 0.56 | 1.10 | 0.13 | 0.46 | 0.05 |
| 1402 | 0.02 | 0.07 | 5.36 | 14.37 | 32.16 | 1.84 | 0.03 | 0.03 | 3.07 | 0.06 | 0.19 | 1.26 | 1.81 | 0.17 | 0.45 | 0.04 |
| 1410 | 0.02 | 0.07 | 8.48 | 17.69 | 34.62 | 2.29 | 0.03 | 0.02 | 1.36 | 0.04 | 0.17 | 0.67 | 1.25 | 0.13 | 0.40 | 0.04 |
| 1461 | 0.06 | 0.06 | 8.38 | 17.22 | 33.60 | 1.74 | 0.07 | 0.02 | 0.63 | 0.03 | 0.81 | 1.79 | 2.85 | 0.28 | 0.74 | 0.06 |
| 1480 | 0.05 | 0.10 | 7.47 | 12.17 | 29.23 | 1.51 | 0.05 | 0.02 | 5.86 | 0.13 | 0.49 | 0.75 | 1.41 | 0.16 | 0.50 | 0.06 |
| 1502 | 0.06 | 0.09 | 7.95 | 12.92 | 29.40 | 1.47 | 0.03 | 0.01 | 2.35 | 0.15 | 0.47 | 1.62 | 2.61 | 0.27 | 0.81 | 0.08 |
| 1532 | 0.03 | 0.05 | 7.65 | 13.67 | 27.45 | 1.47 | 0.03 | 0.01 | 0.36 | 0.59 | 0.26 | 0.33 | 0.58 | 0.06 | 0.19 | 0.02 |
| 1574 | 0.05 | 0.04 | 8.36 | 16.55 | 29.48 | 1.93 | 0.02 | 0.01 | 0.12 | 1.30 | 0.35 | 1.12 | 1.82 | 0.19 | 0.53 | 0.05 |
| 1588 | 0.36 | 0.35 | 13.48 | 15.07 | 27.19 | 2.33 | 0.06 | 0.32 | 1.90 | 1.86 | 0.49 | 0.65 | 1.41 | 0.17 | 0.51 | 0.05 |
| 1612 | 0.06 | 0.09 | 6.52 | 16.30 | 38.86 | 1.32 | 0.04 | 0.05 | 3.34 | 0.49 | 0.39 | 2.00 | 2.78 | 0.27 | 0.69 | 0.06 |
| 1627 | 0.25 | 0.26 | 13.53 | 14.76 | 26.04 | 2.15 | 0.03 | 0.29 | 1.43 | 0.22 | 0.30 | 0.93 | 1.56 | 0.16 | 0.42 | 0.04 |
| 1641 | 0.02 | 0.08 | 11.30 | 15.65 | 28.88 | 2.38 | 0.05 | 0.01 | 0.63 | 0.18 | 0.16 | 0.29 | 0.55 | 0.06 | 0.19 | 0.02 |
| 1649 | 0.05 | 0.71 | 6.69 | 11.81 | 36.17 | 2.08 | 0.08 | 0.34 | 2.14 | 0.24 | 0.23 | 1.08 | 1.57 | 0.15 | 0.38 | 0.04 |
| 1676 | 0.02 | 0.07 | 8.67 | 14.67 | 30.31 | 1.66 | 0.28 | 0.10 | 0.19 | 0.39 | 0.57 | 1.14 | 1.81 | 0.17 | 0.42 | 0.03 |
| 1683 | 0.06 | 0.29 | 6.81 | 15.30 | 25.16 | 1.73 | 0.30 | 0.46 | 2.09 | 0.53 | 0.81 | 1.67 | 2.46 | 0.24 | 0.65 | 0.05 |
| 1692 | 0.06 | 0.21 | 7.40 | 17.60 | 27.45 | 1.48 | 0.10 | 0.40 | 0.75 | 0.99 | 0.83 | 0.91 | 1.70 | 0.17 | 0.44 | 0.04 |
| 1740 | 0.04 | 0.12 | 10.55 | 15.58 | 28.96 | 1.54 | 0.25 | 0.25 | 0.05 | 1.10 | 0.50 | 0.52 | 0.99 | 0.11 | 0.36 | 0.03 |
| 1765 | 0.13 | 0.08 | 9.40 | 12.52 | 35.01 | 1.47 | 0.08 | 0.06 | 2.43 | 0.06 | 0.25 | 1.12 | 2.41 | 0.26 | 0.71 | 0.06 |
| 1776 | 0.03 | 0.03 | 6.71 | 14.40 | 34.55 | 1.30 | 0.11 | 0.02 | 1.64 | 0.62 | 0.24 | 0.91 | 1.52 | 0.16 | 0.46 | 0.04 |

Table DR2. Monazite dating data from the drill cores in Bayan Obo

| sample | Th(ppm) | U(ppm) | Th/U | $^{208}Pb/^{232}Th$ | σ | Pb/Th age(Ma) | σ |
|---|---|---|---|---|---|---|---|
| BO-1 | 2308 | 3.57 | 646 | 0.0462 | 1.7 | 913 | 15 |
| BO-2 | 4197 | 1.03 | 4080 | 0.0438 | 1.7 | 866 | 14 |
| BO-3 | 2506 | 3.04 | 825 | 0.0415 | 1.9 | 822 | 16 |
| BO-4 | 1841 | 2.19 | 839 | 0.0410 | 1.6 | 811 | 13 |
| BO-5 | 2138 | 2.93 | 729 | 0.0401 | 1.6 | 795 | 13 |
| BO-6 | 2056 | 2.60 | 792 | 0.0400 | 1.7 | 792 | 13 |
| BO-7 | 1987 | 2.32 | 858 | 0.0377 | 1.6 | 748 | 12 |
| BO-8 | 2889 | 2.08 | 1389 | 0.0333 | 1.8 | 662 | 12 |
| BO-9 | 1783 | 2.19 | 815 | 0.0318 | 1.9 | 633 | 12 |
| BO-10 | 1436 | 0.97 | 1488 | 0.0288 | 1.9 | 573 | 11 |
| BO-11 | 2294 | 2.56 | 897 | 0.0285 | 1.6 | 569 | 9 |
| BO-12 | 1551 | 1.71 | 907 | 0.0280 | 2.5 | 558 | 14 |
| BO-13 | 1302 | 2.55 | 511 | 0.0266 | 1.6 | 530 | 9 |
| BO-14 | 3134 | 1.58 | 1979 | 0.0259 | 1.6 | 517 | 8 |
| BO-15 | 4817 | 1.32 | 3643 | 0.0224 | 2.2 | 448 | 10 |
| BO-16 | 2654 | <0.1 | >10000 | 0.0206 | 1.6 | 413 | 7 |
| BO-17 | 2407 | <0.1 | >10000 | 0.0206 | 1.7 | 413 | 7 |
| BO-18 | 2230 | <0.1 | >10000 | 0.0206 | 2.0 | 411 | 8 |
| BO-19 | 2934 | <0.1 | >10000 | 0.0205 | 1.8 | 410 | 7 |
| BO-20 | 2307 | <0.1 | >10000 | 0.0204 | 1.8 | 408 | 8 |
| BO-21 | 1709 | 1.68 | 1015 | 0.0203 | 1.6 | 406 | 7 |
| BO-22 | 3272 | 1.42 | 2312 | 0.0197 | 1.8 | 394 | 7 |
| BO-23 | 1482 | 1.83 | 812 | 0.0185 | 1.7 | 370 | 6 |
| BO-24 | 1530 | 1.30 | 1177 | 0.0180 | 1.6 | 361 | 6 |

Table DR3. In-situ Nd isotope of monazites from Bayan Obo drill cores

| sample | $^{147}Sm/^{144}Nd$ | 2σ | $^{143}Nd/^{144}Nd$ | 2σ | age (Ma) | $\varepsilon_{Nd}$ (t)# | $T_{CHUR}$(Ga) |
|---|---|---|---|---|---|---|---|
| BO-1 | 0.04239 | 2 | 0.511362 | 19 | 913 | -6.9 | 1.59 |
| BO-2 | 0.04607 | 5 | 0.511358 | 32 | 866 | -8.3 | 1.63 |
| BO-3 | 0.04606 | 2 | 0.511319 | 22 | 822 | -9.9 | 1.66 |
| BO-4 | 0.04487 | 4 | 0.511348 | 23 | 811 | -9.4 | 1.62 |
| BO-5 | 0.04645 | 4 | 0.511316 | 27 | 795 | -10.5 | 1.67 |
| BO-6 | 0.04651 | 5 | 0.511348 | 22 | 792 | -10.0 | 1.64 |
| BO-7rim | 0.04363 | 8 | 0.511309 | 37 | 748 | -11.3 | 1.65 |
| BO-7rim | 0.04320 | 4 | 0.511305 | 39 | 748 | -11.3 | 1.65 |
| BO-7core | 0.04349 | 6 | 0.511318 | 41 | 748 | -11.1 | 1.64 |
| BO-7core | 0.04633 | 4 | 0.511377 | 25 | 748 | -10.2 | 1.61 |
| BO-8 | 0.04561 | 7 | 0.511372 | 22 | 662 | -11.9 | 1.61 |
| BO-9 | 0.04394 | 2 | 0.511346 | 20 | 633 | -12.9 | 1.62 |
| BO-10 | 0.04507 | 14 | 0.511353 | 25 | 573 | -14.0 | 1.62 |
| BO-11 | 0.04652 | 3 | 0.511346 | 21 | 569 | -14.3 | 1.64 |
| BO-12 | 0.04497 | 4 | 0.511339 | 19 | 558 | -14.5 | 1.63 |
| BO-13 | 0.04375 | 3 | 0.511345 | 24 | 530 | -14.9 | 1.62 |
| BO-14 | 0.04410 | 10 | 0.511341 | 34 | 517 | -15.2 | 1.62 |
| BO-15rim | 0.03962 | 8 | 0.511283 | 38 | 448 | -17.5 | 1.63 |
| BO-15core | 0.04118 | 6 | 0.511326 | 14 | 448 | -16.7 | 1.61 |
| BO-16 | 0.03988 | 3 | 0.511342 | 26 | 413 | -17.0 | 1.58 |
| BO-17 | 0.03938 | 2 | 0.511365 | 25 | 413 | -16.5 | 1.56 |
| BO-18 | 0.03588 | 9 | 0.511334 | 27 | 411 | -17.0 | 1.55 |
| BO-19 | 0.04002 | 11 | 0.511355 | 27 | 410 | -16.8 | 1.57 |
| BO-20 | 0.03950 | 4 | 0.511360 | 23 | 408 | -16.8 | 1.56 |
| BO-21 | 0.04533 | 3 | 0.511362 | 33 | 406 | -17.1 | 1.62 |
| BO-22 | 0.04763 | 20 | 0.511361 | 24 | 394 | -17.4 | 1.64 |
| BO-23 | 0.04527 | 3 | 0.511351 | 27 | 370 | -18.0 | 1.62 |
| BO-24core | 0.04619 | 7 | 0.511377 | 22 | 361 | -17.7 | 1.61 |
| BO-24rim | 0.04616 | 2 | 0.511376 | 23 | 361 | -17.7 | 1.61 |

# $\varepsilon_{Nd}$ (t) values are calculated based on present-day $(^{147}Sm/^{143}Nd)_{CHUR}$ = 0.1967 and $(^{143}Nd/^{144}Nd)_{CHUR}$ = 0.512638.

Table DR4. In-situ trace element compositions (ppm) of dolomite and apatite from Bayan Obo drill cores

| dolomite | | | | | | | | primary | | | | | | | | recrystallization | |
|---|---|---|---|---|---|---|---|---|---|---|---|---|---|---|---|---|---|
| Rb | 0.05 | bdl[#] | bdl | bdl | bdl | bdl | bdl | bdl | 0.09 | bdl | bdl | 0.01 | 0.01 | 0.02 | 0.01 | 0.03 | 0.04 |
| Sr | 1766 | 1528 | 1818 | 2228 | 2174 | 2559 | 2671 | 2429 | 1197 | 2640 | 2738 | 4294 | 4513 | 4378 | 4559 | 4451 | 4289 |
| Ba | 67.5 | 9.34 | 86.1 | 13.4 | 133 | 124 | 561 | 90.1 | 106 | 69.4 | 39.5 | 43.5 | 61.6 | 58.3 | 33.6 | 56.0 | 55.5 |
| Y | 23.3 | 28.8 | 25 | 27.9 | 17.3 | 13.0 | 19.3 | 9.31 | 23.1 | 31.5 | 29.6 | 56.2 | 58.3 | 65.3 | 105.8 | 78.4 | 62.0 |
| La | 7.18 | 3.59 | 9.17 | 4.92 | 5.25 | 5.06 | 9.63 | 3.61 | 15.5 | 65.7 | 27.4 | 36.6 | 36.6 | 56.5 | 109 | 101 | 73.8 |
| Ce | 25.2 | 14.0 | 25.9 | 17.3 | 11.2 | 10.4 | 19.6 | 7.69 | 54.8 | 162 | 62.0 | 128 | 136 | 192 | 362 | 314 | 234 |
| Pr | 3.83 | 2.16 | 3.65 | 2.58 | 1.39 | 1.16 | 2.36 | 0.93 | 7.50 | 15.1 | 7.50 | 17.8 | 19.6 | 26.3 | 51.8 | 43.1 | 31.4 |
| Nd | 16.9 | 11.3 | 16.6 | 13.4 | 5.93 | 5.9 | 11.4 | 4.46 | 32.4 | 65.3 | 33.6 | 77.4 | 85.2 | 112 | 222 | 184 | 136 |
| Sm | 5.03 | 3.37 | 4.10 | 3.94 | 1.52 | 2.67 | 4.69 | 1.81 | 6.54 | 17.1 | 8.94 | 17.9 | 20.4 | 24.8 | 47.3 | 37.0 | 28.4 |
| Eu | 2.03 | 1.60 | 1.99 | 1.71 | 0.73 | 1.15 | 1.79 | 0.84 | 2.47 | 6.35 | 3.36 | 6.52 | 7.67 | 8.64 | 16.3 | 12.5 | 9.60 |
| Gd | 3.99 | 3.48 | 4.12 | 3.73 | 1.75 | 2.46 | 4.45 | 2.44 | 4.79 | 14.5 | 7.22 | 15.3 | 17.5 | 19.6 | 36.8 | 28.1 | 21.7 |
| Tb | 0.90 | 0.81 | 0.76 | 0.69 | 0.42 | 0.41 | 0.95 | 0.40 | 0.85 | 2.24 | 1.30 | 2.84 | 3.38 | 3.68 | 6.45 | 5.0 | 3.92 |
| Dy | 5.61 | 6.23 | 5.31 | 5.16 | 2.82 | 2.86 | 4.75 | 2.26 | 5.17 | 10.3 | 6.85 | 16.2 | 18.1 | 20.1 | 33.7 | 26.1 | 20.1 |
| Ho | 1.16 | 1.32 | 1.23 | 1.24 | 0.79 | 0.53 | 0.92 | 0.36 | 0.90 | 1.69 | 1.28 | 2.8 | 3.0 | 3.38 | 5.5 | 4.11 | 3.23 |
| Er | 2.89 | 4.08 | 3.17 | 3.37 | 1.95 | 1.30 | 1.89 | 0.78 | 2.37 | 3.07 | 3.35 | 5.41 | 5.72 | 6.43 | 10.1 | 7.40 | 5.52 |
| Tm | 0.35 | 0.61 | 0.43 | 0.38 | 0.40 | 0.17 | 0.23 | 0.10 | 0.25 | 0.32 | 0.39 | 0.55 | 0.53 | 0.58 | 0.87 | 0.64 | 0.55 |
| Yb | 2.01 | 3.31 | 2.74 | 2.03 | 2.31 | 0.79 | 1.17 | 0.53 | 1.38 | 1.39 | 2.0 | 2.18 | 2.18 | 2.50 | 3.75 | 2.90 | 2.24 |
| Lu | 0.20 | 0.39 | 0.22 | 0.17 | 0.29 | 0.11 | 0.14 | 0.04 | 0.17 | 0.12 | 0.22 | 0.18 | 0.20 | 0.23 | 0.32 | 0.21 | 0.21 |

Table DR4. continued

| apatite | | | | | primary | | | | | | | recrystallization | |
|---|---|---|---|---|---|---|---|---|---|---|---|---|---|
| Rb | 0.14 | 1.40 | 0.26 | 0.26 | 3.01 | 0.10 | 0.08 | 0.04 | 0.12 | 0.14 | 0.12 | 0.48 | 0.18 |
| Sr | 5109 | 4026 | 5006 | 4586 | 3982 | 2834 | 2663 | 2956 | 2942 | 2364 | 3257 | 3255 | 3223 |
| Ba | 22.9 | 22.7 | 62.4 | 35.3 | 17 | 83 | 94 | 133 | 204 | 78.2 | 64.3 | 66.7 | 223 |
| Y | 1356 | 1153 | 1246 | 1193 | 1107 | 128 | 102 | 121 | 116 | 144 | 183 | 212 | 119 |

| | | | | | | | | | | | | | |
|---|---|---|---|---|---|---|---|---|---|---|---|---|---|
| La | 2133 | 1598 | 1918 | 1553 | 1412 | 158 | 157 | 202 | 241 | 564 | 495 | 846 | 339 |
| Ce | 7601 | 5809 | 6852 | 5646 | 6075 | 585 | 525 | 684 | 779 | 1505 | 1387 | 2372 | 1114 |
| Pr | 1188 | 937 | 1035 | 912 | 1004 | 96.7 | 82 | 104 | 109 | 228 | 187 | 335 | 146 |
| Nd | 5830 | 4406 | 4954 | 4553 | 5151 | 500 | 405 | 516 | 517 | 982 | 827 | 1394 | 647 |
| Sm | 1227 | 902 | 1051 | 947 | 1059 | 106 | 88.4 | 103 | 100 | 161 | 144 | 208 | 116 |
| Eu | 338 | 251 | 287 | 265 | 278 | 26.0 | 21.3 | 25.5 | 24.8 | 37.2 | 35.9 | 49.2 | 27.1 |
| Gd | 800 | 620 | 714 | 675 | 680 | 61.6 | 52.8 | 61.7 | 60.6 | 89.5 | 85.2 | 116 | 67.8 |
| Tb | 102 | 76.6 | 90.0 | 83.5 | 78.7 | 6.75 | 5.6 | 6.55 | 6.05 | 8.35 | 9.24 | 11.5 | 7.06 |
| Dy | 497 | 376 | 451 | 417 | 377 | 36.3 | 29.3 | 34.2 | 31.9 | 40.9 | 49.4 | 58.2 | 33.5 |
| Ho | 72.3 | 54.7 | 65.9 | 61.6 | 53.6 | 5.79 | 4.68 | 5.85 | 5.38 | 6.51 | 8.17 | 9.48 | 5.47 |
| Er | 132 | 102 | 124 | 118 | 99.9 | 13.8 | 10.7 | 12.8 | 12.4 | 14.7 | 19.0 | 22.5 | 12.1 |
| Tm | 11.1 | 8.50 | 10.3 | 9.92 | 8.02 | 1.45 | 1.07 | 1.37 | 1.42 | 1.53 | 1.94 | 2.19 | 1.21 |
| Yb | 38.9 | 30.3 | 37.1 | 36.8 | 28.9 | 6.76 | 5.25 | 6.1 | 6.95 | 7.24 | 8.45 | 10.3 | 5.89 |
| Lu | 3.07 | 2.40 | 2.98 | 3.03 | 2.35 | 0.63 | 0.50 | 0.61 | 0.79 | 0.70 | 0.78 | 0.99 | 0.58 |

[#]below determination limits.

Table DR5. In-situ Sr isotope of dolomite and apatite from Bayan Obo drill cores

| dolomite | | | | apatite | | | |
|---|---|---|---|---|---|---|---|
| primary | | recrystallization | | primary | | recrystallization | |
| $^{87}Sr/^{86}Sr$ | 2σ | $^{87}Sr/^{86}Sr$ | 2σ | $^{87}Sr/^{86}Sr$ | 2σ | $^{87}Sr/^{86}Sr$ | 2σ |
| 0.70250 | 25 | 0.70606 | 33 | 0.70296 | 19 | 0.70351 | 8 |
| 0.70241 | 20 | 0.70669 | 67 | 0.70294 | 17 | 0.70323 | 19 |
| 0.70238 | 22 | 0.70384 | 22 | 0.70293 | 23 | 0.70345 | 13 |
| 0.70271 | 12 | 0.70946 | 53 | 0.70297 | 19 | 0.70349 | 7 |
| 0.70293 | 16 | 0.70760 | 81 | 0.70297 | 34 | 0.70357 | 16 |
| 0.70287 | 9 | 0.70456 | 35 | | | 0.70357 | 18 |
| 0.70290 | 14 | 0.70786 | 50 | | | 0.70367 | 11 |
| 0.70280 | 9 | 0.70682 | 21 | | | 0.70347 | 14 |
| 0.70297 | 10 | 0.70572 | 10 | | | 0.70347 | 12 |
| 0.70284 | 14 | 0.70971 | 19 | | | 0.70364 | 18 |
| 0.70290 | 9 | 0.70889 | 10 | | | 0.70341 | 13 |
| 0.70289 | 4 | 0.70871 | 17 | | | 0.70354 | 13 |
| 0.70281 | 9 | 0.70533 | 14 | | | | |
| 0.70282 | 5 | 0.70568 | 23 | | | | |
| 0.70295 | 8 | 0.70827 | 26 | | | | |
| 0.70294 | 3 | 0.70718 | 35 | | | | |
| 0.70285 | 7 | 0.70467 | 11 | | | | |
| 0.70279 | 4 | | | | | | |